Dependence of level-resolved energy transfer on initial vibrational level in $Li_2 A^1\Sigma_u^+ - Ne$ collisions

Yunxiao Gao, Peter S. Gorgone,[a] Scott Davis,[b] Eric K. McCall,[c] and Brian Stewart
Wesleyan University, Department of Physics, Middletown, Connecticut 06459

(Received 1 September 1995; accepted 17 October 1995)

We have investigated collision induced rotational and vibrational energy transfer in the Li_2 $A^1\Sigma_u^+(v_i, j_i=30) - Ne$ system experimentally under single-collision conditions at an effective temperature of 691 K. Over 800 inelastic rate constants have been measured, with the initial vibrational level v_i ranging from 2 to 24 and $-2 \leqslant \Delta v \leqslant +2$. Increasing v_i results in a linear increase in the vibrational transition rate constants, which is accompanied by a decrease in the rotationally inelastic transition rate constant. The total inelastic rate constant increases with v_i only at the highest values of v_i. Net vibrational energy transfer $\langle \Delta E \rangle$ calculated using rotationally summed rate constants is qualitatively consistent with a simple model. However, explicit inclusion of rotation gives quite different values of $\langle \Delta E \rangle$. The experimental results are compared with our three-dimensional trajectory calculations on an *ab initio* potential surface and on a simple repulsive potential surface. © *1996 American Institute of Physics.* [S0021-9606(96)01404-5]

I. INTRODUCTION

The phenomenon of vibrational energy transfer has many facets. In spite of a history of intensive study that dates to the 1950s and before,[1] numerous aspects of the problem remain to be investigated in detail. In the present study, we explore vibrational transfer over a wide range of reagent vibration at constant reagent rotational angular momentum. Unlike most previous studies, ours has resulted in resolution of both initial and final vibrational and rotational levels. Our results also include detailed measurements of pure rotational energy transfer over the same range of vibrational quantum numbers. In addition to adding detail to what is known about a fundamental molecular collision process, this work constitutes a contribution to a topic receiving much current attention, the collision of molecules at high levels of internal excitation,[2–6] and paves the way for investigations at yet higher levels of reagent vibration. To the best of our knowledge, no similarly detailed investigation has been undertaken previously.

Measurements were made in the system

$$Li_2\ A^1\Sigma_u^+(v_i, j_i=30) + Ne \rightarrow Li_2\ A^1\Sigma_u^+(v_f, j_f) + Ne,$$

with v_i and j_i the initial values of the vibrational and rotational quantum numbers and v_f and j_f their final values. The initial vibrational level was varied from 2 to 24, almost completely spanning the range of v for which published spectroscopic data exist;[7,8] the initial rotational level was held constant at $j_i = 30$.

The choice of lithium dimer was dictated by several considerations. The alkali dimers possess simple, well-characterized structure in their lower excited electronic states, and these states are accessible by optical frequency lasers. Lithium, being the lightest of these, has the widest level spacings, resulting in uncongested dispersed fluorescence spectra that enable us to extract level-to-level inelastic rate constants. The relatively wide level spacings also make the collisions partially vibrationally adiabatic at the temperature of our experiment, placing them in the dynamical regime most relevant for the molecules with wider level spacings whose energy transfer is of practical interest. Perturbations are few, isolated, and largely known,[9] reducing the concern[6] of interference from electronically nonadiabatic effects. Moreover, lithium dimer is the second lightest molecule with a stable ground state at ordinary temperatures and is hence the most tractable theoretically. As a result, one of the few *ab initio* potentials that include the molecular internuclear separation has been calculated for the Li_2 $A^1\Sigma_u^+ - Ne$ system.[10] We have used this potential surface in three-dimensional trajectory calculations for comparison with our experimental results. The A-state lithium dimer – rare gas systems have been subjected previously to investigation of their rotational and vibrational transfer properties,[11–17] and our work contributes to this increasingly comprehensive body of data. Finally, interest in the lithium dimer has increased recently due to its production in photoassociative collisions,[18] and two groups are in the process of determining its vibrational spectroscopy up to the region of the photoassociative data.[19,20] The opportunity now exists for us to continue these studies in future work into the regime where competition with collisional dissociation occurs and interesting long-range effects may become observable.[21]

II. EXPERIMENT

The experiments were carried out using a technique, first employed by Franck and Wood,[22] that uses fluorescence intensities as a measure of excited state populations. The technique has been refined throughout the century, particularly

[a]Present address: Department of Electrical Engineering, University of Washington, Seattle, Washington 98195.
[b]Present address: University of Colorado and Joint Institute for Laboratory Astrophysics, Boulder, Colorado 80309.
[c]Present address: Department of Computer Science, University of Massachusetts, Amherst, Massachusetts 01003.

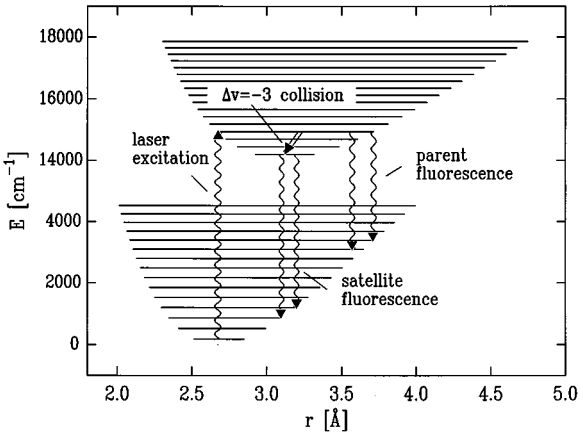

FIG. 1. Experimental concept. Laser excitation of a single vibrotational level in the $A^1\Sigma_u^+$ state results in *parent line* emission from the laser populated level and *satellite line* emission from collisionally populated levels. The satellite to parent intensity ratios are related to the level-to-level rate constants through a Stern–Volmer analysis.

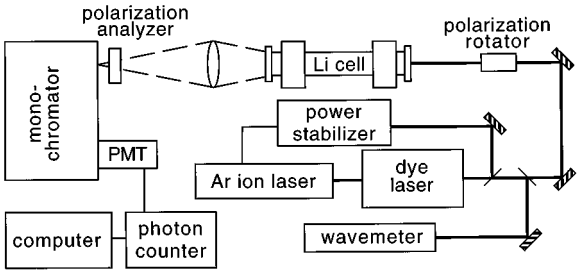

FIG. 2. Experimental arrangement. A single-frequency cw dye laser excites lithium molecules in a heated cell containing neon gas. Fluorescence is imaged into and dispersed by a double monochromator, making possible the identification of parent and satellite lines and measurement of their intensities.

subsequent to the development of narrow bandwidth lasers;[12,15,23,24] as currently implemented, it uses the excited state lifetime to establish single-collision conditions. Our version of the technique is similar to that of Magill *et al.*;[15] a brief description has been given previously.[17] A single vibrotational level in the excited state is populated with a dye laser. The dispersed fluorescence signal contains strong *parent lines* that emanate from laser-populated levels, and weaker *satellite lines* that emanate from collisionally populated levels. Variation of the target gas pressure results in variation in the satellite line intensities. These intensities, after correction for line strength and instrument response, are taken as measures of the excited state population densities; analysis of the pressure dependence then yields the level-resolved rate constants. The experimental concept is shown in Fig. 1.

A. Data acquisition

The equipment arrangement is shown in Fig. 2. Lithium metal and neon gas were placed in a stainless steel cell. The cell is a 16 in. stainless steel tube, 2 in. in diameter, that has flanges welded to its ends to hold the optical windows in place. A cartridge heater (ARI Industries) wound around the center of the cell establishes a hot zone that is uniform over the central 1.5 cm region, a length approximately equal to the depth of focus of the lens used to image fluorescence into the monochromator. Three inch water cooled zones at either end of the cell cool the lithium and buffer gas, resulting in condensation of the lithium before it reaches the windows. A stainless steel mesh that lines the cell returns condensed lithium to the hot zone at its center. This arrangement makes it possible to operate the cell for periods in excess of a year without the need to open it to replenish the lithium. The cell temperature was maintained at 898.0 ± 0.1 K with a Eurotherm model 91 temperature controller. The vapor pressure of atomic lithium at 898 K is 0.0918 torr, and the vapor pressure of lithium dimer is 1.47×10^{-3} torr.[25] The neon pressure was varied from 0.6 to 3.0 torr to enable us to carry out a pressure analysis to obtain the rate constants. The range of pressures was chosen so that the neon pressure was always substantially in excess of the lithium pressure, preventing the establishment of heat pipe conditions.[26] Pressure was determined by use of a Baratron capacitance manometer.

A single vibrotational level in the Li_2 $A^1\Sigma_u^+$ electronically excited state was populated by a Spectra-Physics 380D single-frequency cw dye laser. This level was carefully chosen to minimize off-resonant excitation of other levels whose fluorescence, though weak, would interfere with our analysis of the very small vibrationally inelastic satellite lines. A Spectra-Physics model 373 power stabilizer was used to maintain a constant excitation rate. Power densities were maintained at low levels (typically around 10 mW/cm^2) to prevent saturation of the transition; measurement of a parent line signal as a function of laser power before the experiment enabled us to operate at the highest power that gave a linear response. The polarization of the emission was analyzed at an angle of 54.7° with respect to the polarization of the incident radiation[27] to eliminate alignment effects. Signal was maximized by setting the analyzer angle to give the greatest monochromator signal and rotating the laser polarization with respect to the analyzer by means of a double Fresnel rhomb. Three dyes, DCM, Kiton Red, and Rhodamine 6G, spanned the range of excitations needed. The lowest v' could be reached from $v'' = 0$, but poor Franck–Condon overlap necessitated exciting from higher v'' for the higher values of $v' = v_i$, reducing signal and limiting the dynamic range of the measurements.

The emission was dispersed in a SPEX 14018 double monochromator. With a slit width of 50 μ, the resolution was 0.3 cm^{-1}. Photoelectric detection with an RCA C31034 photomultiplier tube and photon counting using a Stanford Instruments SR400 photon counter were employed to determine line intensities; particular care was taken to optimize discriminator levels and to reduce stray light in an effort to achieve the maximum possible dynamic range in our measurements of the small vibrationally inelastic rate constants. The monochromator was scanned nonlinearly so that a constant number of data points was collected for each line. The

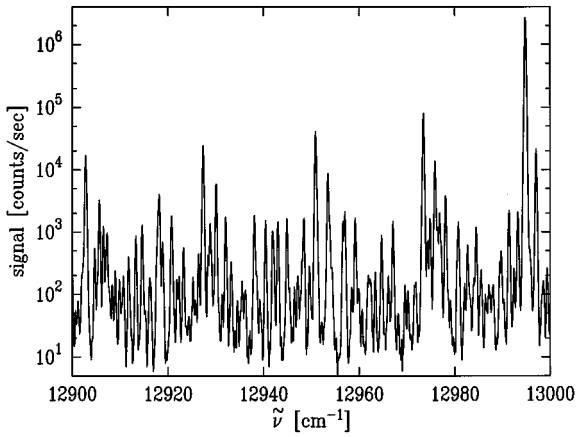

FIG. 3. Dispersed fluorescence spectrum at a total pressure of 1.0 torr for $v_i = 2$. An intense parent line is visible, as are satellite line progressions due to rotationally inelastic collisions. The smaller lines, 1000 counts per second or less in size, are due to the vibrationally inelastic collisions that are of primary interest in this study. The noise level, due to dark counts and scattered light, is about ten counts per second. Most of the lines shown have been assigned, although blended lines were excluded from the analysis.

highest three of these were summed as a measure of the line intensity.[15] A typical scan range was 200 cm^{-1}, long enough to include at least one parent line to determine the absolute wave-number scale for the scan. Dwell times of 0.5–1.0 s were used. Before and after each scan, both the laser frequency and intensity were checked by monitoring and maximizing the fluorescence signal from one parent line. A portion of an experimental scan is shown in Fig. 3. Enough scans were taken to cover several of the strongest vibrational bands, with the result that multiple determinations of many rate constants could be made from the several lines emanating from a given excited state level. Scanning over several bands also increased the chance that a very small line corresponding to a very small rate constant appeared at least once in the spectrum without interference from larger nearby lines.

B. Data analysis

To obtain measures of the excited state population densities, it was necessary to normalize the fluorescence signal by instrument response and line strength. This normalization entailed computing j-dependent vibrational bandstrengths, including the r-dependence of the electronic transition moment. The potential is well known for $v' \leqslant 26$ (Refs. 7 and 8) and the transition moment has been measured and calculated (see, e.g., Refs. 28 and 29), facilitating these calculations. The parent line intensities themselves, after normalization by the vibrational bandstrengths and Hönl–London factors, were used to determine the wave-number dependence of the instrumental response.

Experimental scans were taken over a sufficient range that many vibrational bands were observed. This enabled us to glean enough unblended lines to determine many of the very small vibrationally inelastic rate constants for $\Delta v = \pm 2$. The rate equation for the final level population density

$$\frac{dn_f}{dt} = k_{if} n_i n_{\mathrm{Ne}} - \Gamma_f n_f \tag{1}$$

then gave, in steady state, the absolute level-resolved rate constants k_{if} from the excited state lifetimes Γ_f and the pressure dependence of the population density ratios n_f/n_i. In practice, we added to Eq. (1) terms representing multiple collisions and collisions with lithium atoms in order to improve the accuracy of our rate constants.[15] In cases where we had intensities from multiple transitions originating from a given excited state level, the data were averaged after correction for line strength and instrument response, but before the pressure fit was used to extract the rate constants.

The excited state lifetime is 18.5 ± 0.5 ns over the experimental range of v_i.[9,30] A cubic fit to the lifetime as a function of term energy was used to remove most of the small systematic variation. A very few excited state levels were accidentally predissociated by coupling with the $b\ ^3\Pi_u$ state,[30,31] necessitating corrections to their lifetimes. Also, competition from collisional dissociation required consideration. The rate constant for collisional dissociation in this system for $v_i = 15$, $j_i = 21$ has been determined to be $6.1 \pm 1.2 \times 10^{-15}$ cm^3 s^{-1},[32] an order of magnitude smaller than the smallest of our measured rate constants. This rate constant was determined at a temperature of 908 K. Using the approximate scaling suggested by Ennen and Ottinger,[32] we estimate a cross section of 2.0×10^{-14} cm^3 s^{-1} for $v_i = 24$ at our experimental effective temperature of 691 K. This is smaller than any level-resolved rate constant at that value of v_i, and hence is negligible. However, collisional dissociation will increase rapidly in importance at higher values of v_i and will need to be considered in future work.

Because the molecules were excited at line center, the distribution of collision velocities was not a Maxwell–Boltzmann distribution. One velocity component of the Li_2 molecule was frozen out, resulting in a relative velocity distribution of the form[13] (in units of $\sqrt{kT/m_{\mathrm{Li}_2}}$)

$$df = \frac{v e^{-v^2/2(\alpha+1)}}{\sqrt{\alpha+1}}\ \mathrm{erf}\left(\frac{v}{\sqrt{2\alpha(\alpha+1)}}\right) dv, \tag{2}$$

where α is the mass ratio $m_{\mathrm{Li}_2}/m_{\mathrm{Ne}}$. This distribution is nevertheless very similar to a Maxwell–Boltzmann distribution ($df = \sqrt{2/\pi} v^2 e^{-v^2/2} dv$ in the same units) at an effective temperature;[12] we found $T_{\mathrm{eff}} = 690.8$ K from a least-squares fit to the true distribution.[17] The distribution of Eq. (2) is a bit lower at its maximum than the best-fit Maxwell–Boltzmann distribution, and a little higher in the exponential tail. Although the fit is quite close in the present case, the distributions can differ significantly when the mass ratio α is small, and in any event it is necessary to use the effective temperature rather than the cell temperature in reporting rate constants derived from molecules excited with a narrow bandwidth laser. The average relative velocity of the colli-

sions at this effective temperature is 1.33×10^5 cm s^{-1}, corresponding to a collision energy of 611 cm^{-1}. The mean collision energy is 720 cm^{-1}.

Error estimates reported with the rate constants include easily determined statistical effects such as photon counting noise and standard errors from pressure fits and multiple rate constant determinations. The actual uncertainties in the data are somewhat larger, but are difficult to quantify. Effects such as spectral overlap and imperfect knowledge of the vibrational band strengths contribute to the uncertainty to an increasing degree as the size of the rate constants declines. Based upon the observed scatter in the rate constants determined from multiple bands and also on the use of different functional forms for the pressure dependence, we estimate that the quoted uncertainties for rate constants larger than 1×10^{-12} cm^3 s^{-1} should be augmented by 5% of the rate constant at low v_i and 10% or more at high v_i. The absolute error estimate climbs as the rate constants decline, and should probably be regarded as 50% below 1×10^{-13} cm^3 s^{-1}.

III. CLASSICAL TRAJECTORY CALCULATIONS

We have computed rate constants from quasiclassical trajectories for comparison with our experimental data. We used a fast action-angle variable algorithm,[33] which assumes that Li_2 $A^1\Sigma_u^+$ is bound by a potential of the form

$$U(r)=\frac{1}{2}\mu\omega^2 r_0^2\left(\frac{r-r_0}{r}\right)^2, \tag{3}$$

where r is the molecular internulear separation and r_0 its equilibrium value, μ is the reduced mass of the Li_2 molecule, and ω is its vibrational frequency. This simple potential approximates very closely the empirical Li_2 $A^1\Sigma_u^+$ RKR potential determined spectroscopically by Kusch and Hessel[7] for $v_i\leqslant25$.[33] Calculations were carried out on potential surfaces of the form $V(R,r,\cos\gamma)$, where R is the atom–diatom separation, r the diatom internuclear separation, and γ the angle between the rotor axis and the line connecting the atom and diatom centers of mass. Calculations typically consisted of 20,000 trajectories at each of eight velocities, chosen to correspond to the first eight points of a 15 point Gauss–Laguerre integration[34] over the Maxwell–Boltzmann velocity distribution at the effective temperature of 691 K. Level-to-level cross sections were determined by the standard histogram method.[35] Rate constants thus determined agree with those obtained by integrating over the exact velocity distribution of Eq. (2) to within a few percent for all but the smallest rate constants.[17]

A. The Alexander–Werner *ab initio* potential

Alexander and Werner have obtained an *ab initio* potential energy surface for the Li_2 $A^1\Sigma_u^+$ – Ne system[36,10] from a multireference configuration interaction calculation. The range of internuclear separations r is somewhat limited, including the r values 2.672, 3.108, and 3.493 Å, the second of these values being the equilibrium internuclear separation. The inner and outer turning points for Li_2 $A^1\Sigma_u^+$ at $v=2$ are 2.805 and 3.482 Å, so the potential is near the limit of the range of validity of its input data for this value of v. The Alexander–Werner potential has been used previously in quantum mechanical calculations of rotationally[10,36] and vibrationally[36] inelastic scattering. The rotationally inelastic calculations agreed very well with experimental rate constants[12] and velocity dependent cross sections[13] even though these calculations were carried out at $v_i=9$, beyond the range of the potential input data. We find the potential to be reasonably well behaved in trajectory calculations up to at least $v_i=7$, although an increasing number of trajectories fail at the highest energies as v_i increases. Collisions at these energies make a very small contribution to the rate constants. We have reported previously classical trajectory calculations using this potential surface with $v_i=2$.[17]

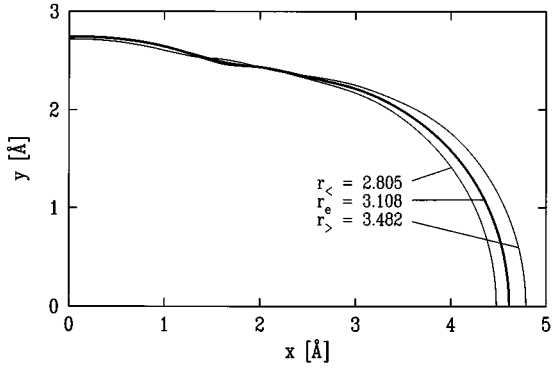

FIG. 4. Equipotentials of the Alexander–Werner *ab initio* potential surface at a collision energy of 720 cm^{-1}, the mean collision energy of our experiment. The heavy line is the equipotential for $r=3.108$ Å, the equilibrium internuclear separation. The thin lines give the equipotentials for $r=2.805$ Å and $r=3.482$ Å respectively, the inner and outer turning points of the lithium dimer for $v=2$.

Figure 4 shows 720 cm^{-1} equipotentials of the Alexander–Werner potential for its equilibrium internuclear separation as well as the $v=2$ inner and outer turning points. It is apparent that the potential is extremely anisotropic: its expansion in Legendre polynomials required inclusion of terms through $P_{18}(\cos\gamma)$.[10] Similarly extreme potential anisotropy has been noted previously in the Li_2 $A^1\Sigma_u^+$ - He system.[37] It is also interesting to observe that the bulk of the change in the potential due to the variation of r occurs at angles less than 45° from the molecular axis. This potential surface resembles ground state alkali dimer – rare gas potentials[38,39] in its R-dependence, but is substantially more anisotropic.

B. Exponentially repulsive model potential

Because the Alexander–Werner potential cannot be used at high v_i, we employed a simple model potential to explore the dynamics throughout the measured range of v_i. More importantly, use of this simple potential also enables us to determine which features of the observed rate constant distributions can only be mo deled using a realistic potential and which can be modeled using a generic potential.

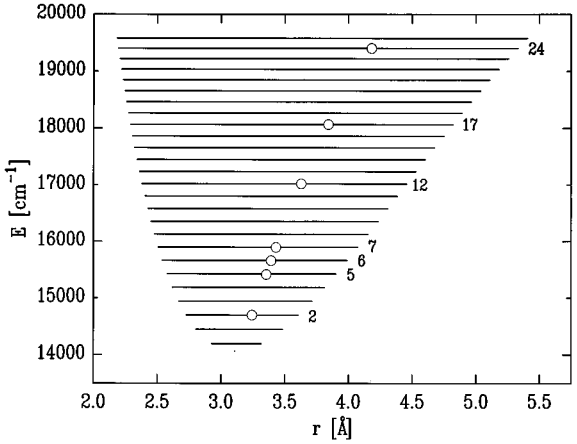

FIG. 5. The vibrational levels of Li_2 $A^1\Sigma_u^+$ (Refs. 7 and 8). The open circles indicate the vibrational levels for which we have made measurements and are located at the expectation value of the internuclear separation $\langle r \rangle$ for their respective levels.

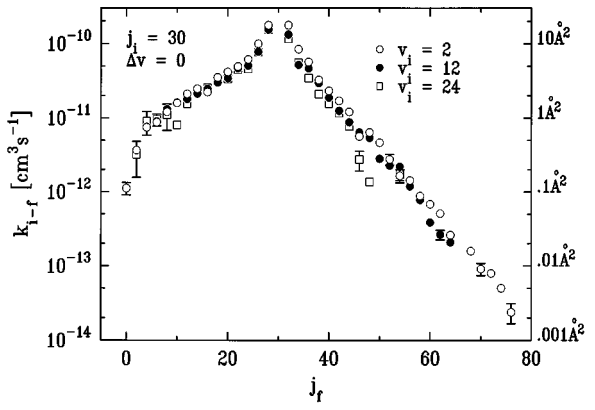

FIG. 6. Measured vibrationally elastic ($\Delta v = 0$) rate constants as a function of final rotational quantum number j_f for $v_i = 2$, 12, and 24, and $j_i = 30$. The scale at the right gives the corresponding thermal cross section size, obtained by dividing the rate constant by the mean thermal velocity.

Using a simple exponentially repulsive (Born–Mayer) potential of the form $V = Ae^{-R/L}$ for the lithium atom – neon atom interaction, and treating the three-body potential as a simple sum of two-body potentials, we have

$$V = Ae^{-r/2L}[e^{-R_a/L} + e^{-R_b/L}], \tag{4a}$$

$$R_a = \left(R^2 + \frac{r^2}{4} - rR\cos\gamma\right)^{1/2}, \tag{4b}$$

$$R_b = \left(R^2 + \frac{r^2}{4} + rR\cos\gamma\right)^{1/2}, \tag{4c}$$

where R_a and R_b are the distances from neon to the two lithium atoms. In this formula, we have assumed that the interaction of the more distant lithium atom with the neon may be neglected. After adjusting the parameters, we found our data best reproduced with $A = 1.2\times10^7\text{cm}^{-1}$ and $L = 0.5$ Å.

IV. RESULTS AND DISCUSSION

The RKR potential for $^7Li_2$ $A^1\Sigma_u^+$ (Ref. 7) is shown in Fig. 5; levels for which we have taken experimental data are indicated. At $v_i = 24$, the highest v_i for which we have data, the vibrational energy is 57% of the dissociation energy. The potential is not very anharmonic in the region of our data; the vibrational spacing declines from 249 cm^{-1} at $v_i = 2$ to 181 cm^{-1} at $v_i = 24$, with the point of inflection in the outer turning point occurring around $v = 17$. Also indicated in Fig. 5 is the expectation value of the internuclear separation, which increases from 3.24 to 4.18 Å over the range of v_i studied. It is not known how many vibrational levels the A state has, but the number has been estimated[21] to be 105 for $^6Li_2$, corresponding to 113 for $^7Li_2$. The large number results from the shallow long range $1/R^3$ potential, which supports many closely spaced vibrational levels with large outer turning points. Thus the remaining 43% of the potential contains nearly four fifths of the vibrational levels.

We have measured more than 800 inelastic rate constants in the seven vibrational levels $v_i = 2,5,6,7,12,17$, and 24, of which over 600 are vibrationally inelastic. The initial rotational quantum number j_i is equal to 30 for all values of v_i. The rate constants span more than four orders of magnitude and include the particularly well determined rate constants for $v_i = 2$ that were the subject of our recent detailed comparison with calculations on the Alexander–Werner potential.[17] Tables of individual level-to-level rate constants have been deposited with the AIP Physics Auxiliary Publication Service (PAPS).[40]

A. Rotationally inelastic rate constants

Figure 6 shows the j_f distribution of purely rotationally inelastic (vibrationally elastic) rate constants for $v_i = 2$, 12, and 24. The rate constants are consistent with previously measured rate constants with $v_i = 9$ and $j_i = 22$ and 42.[12] The change in the distribution with increasing v_i is very slight, although it is clear that there is a small decline in the overall size of the rate constants as v_i increases. In an attempt to discern any variation in the shape of the distributions, we have carried out a fit using the energy-corrected sudden (ECS) fitting law of DePristo *et al.*[41] The matrix of rate constants $\{k_{j_i\to j_f}\}$ is generated from an array of basis rate constants $\{k_{j\to 0}\}$ through the scaling relation

$$k_{j_i\to j_f} = (2j_f+1)e^{-(E_>-E_i)/kT}\sum_j (2j+1) \times \begin{pmatrix} j & j_i & j_f \\ 0 & 0 & 0 \end{pmatrix}^2 A(j,j_>)k_{j\to 0}, \tag{5}$$

where $j_>$ is the larger of j_i and j_f, T is the temperature, ( ) is a 3-j symbol, and $A(j,j_>)$ is an adiabatic factor given by

$$A(j,j_>) = \frac{1+\tau_j^2/6}{1+\tau_{j_>}^2/6}. \tag{6}$$

It is this adiabatic factor that makes ECS scaling differ from infinite-order sudden (IOS) scaling. The scaled collision du-

ration $\tau_j = \omega_j T_d$, with ω_j the rotational angular frequency of the molecule and T_d the collision duration, gives the number of radians the molecule rotates during a collision. This may be approximated as

$$\tau_j = 4\pi c B j \ell_c / \bar{v}, \tag{7}$$

where B is the molecular rotation constant, c is the speed of light, $\bar{v}$ is the average collision speed, and ℓ_c is a length characteristic of the atom–diatom interaction. The physical significance of this characteristic length is not well defined, but ℓ_c has been interpreted as the average impact parameter for rotationally inelastic collisions.[41] A fit of the ECS fitting law to data results in a determination of this parameter.

A complete fit to the data can be obtained by employing the exponential-power (EP) expression for the basis rate constants

$$k_{j\to 0} = a[j(j+1)]^{-\gamma} e^{-(j/j^*)^2}, \tag{8}$$

where a, γ, and j^* are parameters determined from the fit. The ECS fitting procedure, in conjunction with the above exponential-power law expression for the basis rate constants, has proved quite successful in modeling large quantities of rate constant data for lithium–rare gas collisions with a single value of v_i.[12]

Application of the ECS-EP relations to our data was complicated by the fact that the fit parameters are quite sensitive to the range of j_f in the data, which differs for each v_i. It was nevertheless possible to discern an increase in the length parameter ℓ_c with increasing v_i, consistent with an increase in the average moment arm due to the increasing mean molecular anisotropy. This implies that the global ECS fitting that has been employed previously[13] is not applicable over a range of quantum numbers that includes substantial variation in the average internuclear separation. Thus, global ECS scaling may also break down for a data set including a large range of j_i, since the mean internuclear separation increases with j due to centrifugal distortion. We also obtained the ℓ_c parameter from ECS-EP fits to rate constants resulting from trajectories on the Alexander–Werner potential. Although the range of validity of this potential is restricted, the ℓ_c values from fits to calculated rate constants are entirely consistent with the experimental results. The experimental and computed values of ℓ_c are shown in Fig. 7.

The variation in the total (rotationally summed) rotationally inelastic rate constant $k_{\Delta v=0}$ with the initial vibrational level is subject to two competing influences. As v_i increases, many collisions that are vibrationally elastic at low v_i become vibrationally inelastic; the bulk of these collisions come at the expense of the purely rotationally inelastic channel, resulting in a reduction of $k_{\Delta v=0}$. On the other hand, the increase in the molecular length results in an overall increase in the collision rate constant, and an increase in the rotationally inelastic rate constant in particular due to the attending increase in molecular anisotropy. The outcome of this competition will be determined by the collision energy and details of the potential energy surface. We have obtained total rotationally inelastic rate constants by summing over all j_f for a given v_i and j_i (see Table I). This necessitated interpolating a small number of missing rate constants; the interpolations were carried out by inspection. We find that $k_{\Delta v=0}$ decreases by about 25% as v_i increases from 2 to 24.

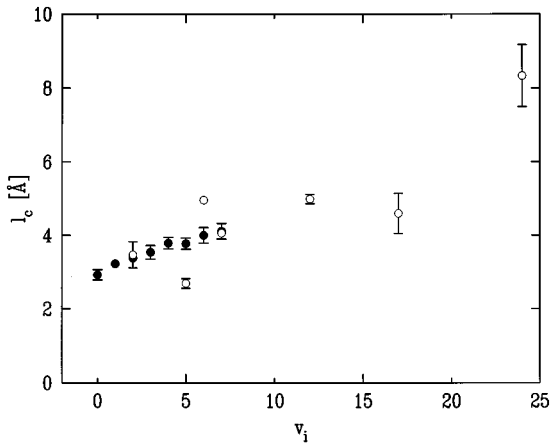

FIG. 7. Length parameters ℓ_c from ECS fits to the vibrationally elastic rate constant distributions. The open circles are from fits to experimental data, and the filled circles are from fits to rate constants obtained from quasiclassical trajectory calculations on the Alexander–Werner *ab initio* potential surface.

Other experimental work examining the dependence of rotational transfer on initial vibration is sparse. Yang and Wodtke[42] examined rotational transfer in collisions of NO with itself. They changed v_i from 8 to 19, adding 2 eV of vibrational energy to the NO molecule, but could discern no systematic effect of the vibration on individual or total rotationally inelastic rate constants. They placed an upper limit of 20% on the possible variation in the total rotationally inelastic rate constant. Barnes *et al.* compared rotational transfer in HF – Ar with $j_i=2$ at $v_i=1$ and 2,[43] finding no significant effect except perhaps a small increase in the cross section for $\Delta j = \pm 1$ with increasing v_i.

Rubahn[44] calculated total rotationally inelastic cross sections as a function of v_i for the Na_2 $X^1\Sigma_g^+$ – Ne system at collision energies of 1, 10, and 100 meV via quasiclassical trajectories on a semi-empirical potential surface.[45] The cross section rises with v_i at each of these energies, sharply at 1 meV and almost not at all at 100 meV. This latter collision energy is most similar to our average collision energy of 89 meV. On examining the velocity dependence of the rotationally summed cross sections resulting from classical trajectories on the *ab initio* potential surface, we find the same behavior. At still higher collision energies, the trend is reversed, with increased vibration leading to a decline in the rotationally inelastic cross section. This results from the steep increase in the vibrationally inelastic cross section at the higher collision energies, which withdraws flux from the purely rotationally inelastic channels. The crossover point is almost exactly at the mean thermal velocity of our experiment. The slight decline we observe results from the preferential weighting of larger velocities in the velocity averaged rate constant and from the fact that the cross sections for different v_i are similar just below $v_{\mathrm{rel}}=1.3\times 10^5$ cm s^{-1} but diverge

TABLE I. The rotationally summed rate constants $k_{\Delta v}$, determined from the experimental rate constant distributions. Statistical uncertainties are given in parentheses; the true uncertainties are larger (see text). Results in brackets are estimates; the total rate constants k_V and k_{total} for $v_i=17$ and 24 are lower bounds, including the estimates shown but excluding higher values of Δv, which may contribute substantially.

v_i	k_{-2}	k_{-1}	k_0	k_1	k_2	k_V	k_{total}
2	0.76(0.01)	3.46(0.05)	102.1(1.2)	2.44(0.04)	0.40(0.01)	7.25(0.06)	108.4(1.0)
5	1.49(0.02)	6.24(0.04)	96.1(1.5)	3.77(0.05)	0.70(0.02)	13.4(0.2)	109.4(1.7)
6	2.38(0.04)	6.75(0.09)	89.8(1.7)	4.43(0.06)	0.88(0.04)	16.1(0.2)	105.9(1.9)
7	2.48(0.13)	7.48(0.17)	91.2(3.6)	4.88(0.05)	0.96(0.04)	17.5(0.2)	108.4(3.8)
12	3.72(0.06)	10.29(0.12)	84.0(1.2)	7.57(0.12)	1.26(0.02)	25.8(0.2)	109.8(1.4)
17	5.96(0.10)	12.96(0.18)	90.7(2.8)	9.24(0.18)	[1.7]	>29.9	>120.6
24	[7.6]	17.84(0.65)	76.4(0.9)	14.07(0.82)	[2.3]	>41.8	>118.2

rapidly above this velocity. The computed velocity dependence of the total rotationally inelastic cross section is shown in Fig. 8 for several values of v_i.

B. Vibrationally inelastic rate constants

Representative vibrationally inelastic rate constant distributions are shown in Fig. 9 for several values of v_i. Tables containing all the experimental level-resolved rate constants are given in the supplementary material.[40] At $v_i = 2$, the largest vibrationally inelastic rate constant is about 2×10^{-12} cm^3 s^{-1}, just 1% the size of the largest rotationally inelastic rate constant at the same v_i. The smallest measured rate constant is about 5×10^{-14} cm^3 s^{-1}, corresponding to an average level-to-level cross section of 0.004 Å^2. Experimental and computed rate constant distributions for $v_i = 7$ are shown in Fig. 10. The agreement between trajectory calculations on the *ab initio* surface and experimental rate constants for $\Delta v = -1$ is nearly quantitative, with the calculated distributions slightly narrower than the experimental distributions. But the model potential does quite a good job also, perhaps even better for $\Delta v = +1$ than the *ab initio* potential. However, it fails to capture the shift in the peak of the $\Delta v = -1$ distribution. A similar comparison of calculations with experimental data for $v_i = 2$ can be found in Ref. 17.

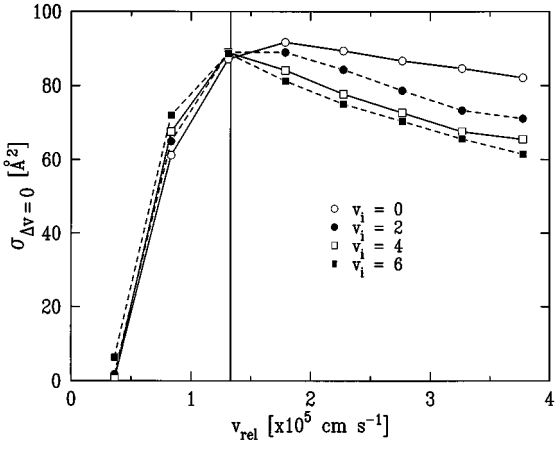

FIG. 8. Velocity dependence of the total rotationally inelastic cross section for several values of v_i. Cross sections were calculated from quasiclassical trajectories on the *ab initio* potential surface and were summed over j_f. The vertical line indicates the mean thermal velocity of the experiment.

1. j_f distributions

Examination of the rate constant distributions of Fig. 9 reveals several trends with increasing v_i. First, the overall magnitude of the rate constants increases with increasing initial vibrational excitation. This well-known phenomenon will be discussed in the following section on rotationally summed rate constants. Second, the peak of the rate constant distribution is shifted sharply away from j_i for negative values of Δv but barely or not at all for positive values of Δv. Third, the distribution of final rotational levels is superficially similar for all v_i, although detailed analysis reveals systematic changes with increasing vibration.

The systematic shift of the peak away from j_i for $\Delta v=-1$ is reminiscent of the behavior seen in this system at higher j_i.[14] For $j_i = 44$–76, the peak of the vibrationally inelastic rate constant distribution is shifted away from j_i according to the rule

$$\Delta j^{\text{peak}} = -4\Delta v. \tag{9}$$

This rule coincides at $j_i = 64$ with the criterion for intramolecular energy conservation

$$\frac{\Delta j^{\text{peak}}}{\Delta v} \simeq -\frac{\omega_v}{2B_v j_i}; \tag{10}$$

its persistence at other j_i has led to the term ''quasiresonant V-R transfer'' for this phenomenon. The phenomenon is further characterized by very narrow j_f distributions and an enhancement of the vibrationally inelastic cross section at low velocity. The rate constants are very large, entirely dominating the energy transfer process by $j_i = 64$. Moreover, Eq. (9) is valid at these high values of j_i for $-3\leqslant\Delta v\leqslant2$. The phenomenon has been subjected to a variety of analyses.[36,46–49] The most important factor in its onset is that the rotational frequency is comparable to the vibrational frequency, enhancing collisional coupling of these two degrees of freedom.

In the present case of $j_i = 30$, not all the conditions for efficient V–R transfer are present. The frequency ratio of Eq. (10) varies little as v_i increases from 2 to 24, changing from

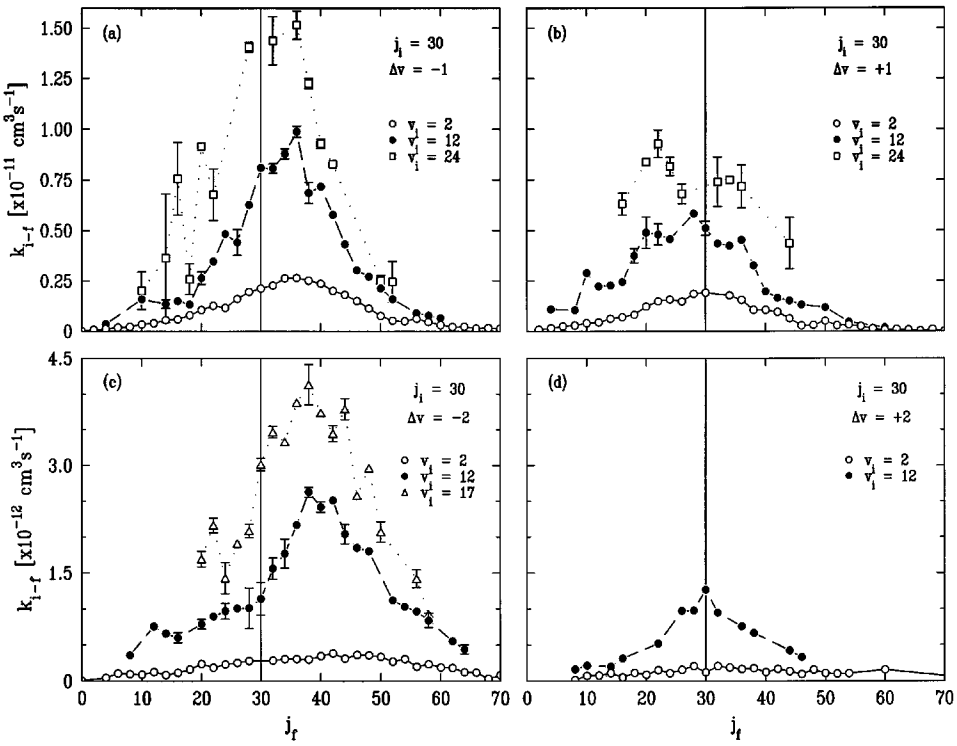

FIG. 9. (a) Measured vibrationally inelastic rate constants with $\Delta v = -1$ as a function of the final rotational quantum number j_f for $v_i = 2$, 12, and 24, and $j_i = 30$. The vertical line indicates the rotationally elastic channel. The connecting lines are to guide the eye only. (b) Measured vibrationally inelastic rate constants with $\Delta v = +1$ as a function of j_f for $v_i = 2$, 12, and 24. (c) Measured vibrationally inelastic rate constants with $\Delta v = -2$ as a function of j_f for $v_i = 2$, 12, and 17. Note the change in ordinate scale. (d) Measured vibrationally inelastic rate constants with $\Delta v = +2$ as a function of j_f for $v_i = 2$ and 12.

8.45 to 8.02. This ratio is twice the ratio at $j_i = 64$, and the rotational frequency is apparently not sufficiently near the vibrational frequency in the present instance for the strong coupling necessary for quasiresonant V–R transfer to occur. The shift observed in the $\Delta v = -1$ distribution is about 6 $\hbar$, less than that predicted by energy resonance, but still consistent with the idea of quasiresonance. However, as can be seen in the data shown in Fig. 9, the shift is essentially absent in the $\Delta v = +1$ case. The same observations hold for $\Delta v = \pm 2$, although the data for $\Delta v = +2$ are limited.

Another distinguishing feature of quasiresonant V–R transfer is absent here: its independence of the atom–molecule interaction potential. At higher j_i, the interaction potential was found to have little effect on the shape of the j_f distributions.[14,15] The experimental evidence for this observation was the similarity of the distributions for target gases ranging from Ne to Xe. The Li_2 – Xe potential should have a deep well owing to the large polarizability of the Xe atom, whereas the Li_2 – Ne potential does not. The computational evidence was that even a simple ''breathing ellipsoid'' potential function – which bears little resemblance to the Alexander–Werner potential – gave rate constant distributions similar to those measured, with peaks having the same locations and comparable widths. The rate constant distributions calculated from classical trajectories on the Alexander–Werner *ab initio* potential surface resemble our results closely in all respects except overall size (see Fig. 10 and Ref. 17); in particular they reproduce the shift for the $\Delta v = -1$ rate constants and its absence for the $\Delta v = +1$ rate constants. However, calculations on the simple exponential potential give little or no shift for either value of Δv. We conclude that the case of $j_i = 30$ in this system is too low to induce the strong vibration–rotation coupling that is characteristic of quasiresonant V–R transfer, although it is high enough to display some of its features and should probably be regarded as marking the onset of a transition to the regime of efficient coupling.

The rotational level distributions of the vibrationally inelastic rate constants appear quite similar in shape for the different initial vibrational levels. Attempts to scale them to one another, however, reveal that the $\Delta j < 0$ portion of the distribution rises faster with increasing v_i than the $\Delta j > 0$ portion. We observe this phenomenon in both our experimental rate constants and in rate constants calculated on the *ab initio* potential.

2. Dependence on v_i

The role of initial vibration in determining the overall scale of vibrational transfer can best be examined by comparing rate constants summed over j_i. Forming these sums necessitated some interpolation and extrapolation of missing data, which was accomplished by inspection. The substantial uncertainties in the extrapolated data were offset for the most

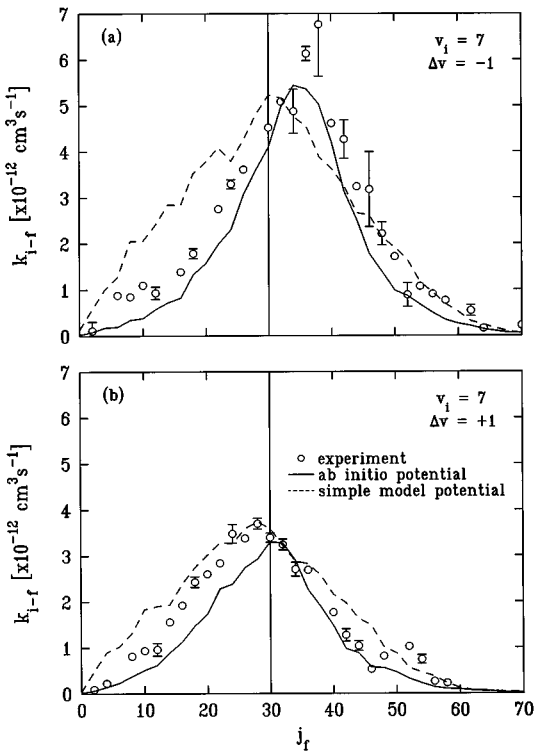

FIG. 10. A comparison of vibrationally inelastic rate constants for $v_i = 7$ and $j_i = 30$. Open circles: experimental results; solid line: results of quasiclassical trajectories on the *ab initio* potential surface; dashed line: results of trajectories on a simple exponentially repulsive model potential surface for (a) $\Delta v = -1$, and (b) $\Delta v = +1$.

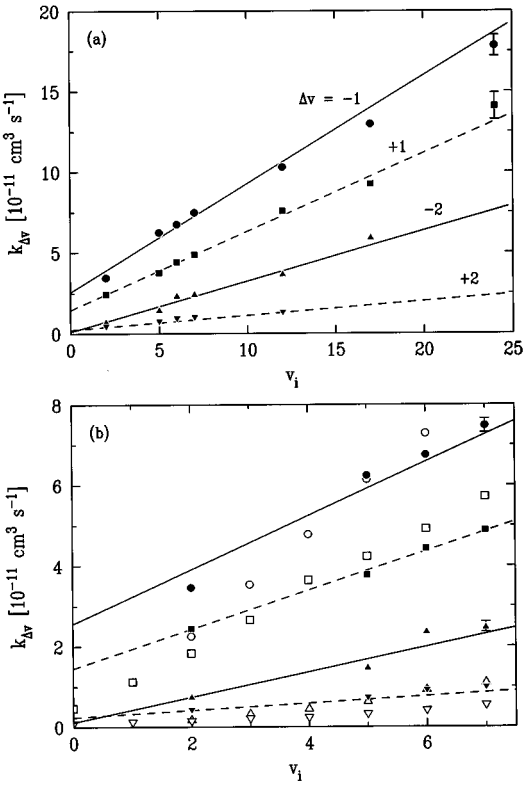

FIG. 11. The total (rotationally summed) vibrationally inelastic rate constants as a function of v_i (from Table I). (a) Rate constants for $\Delta v = \pm 1$ and ± 2 over the entire measured range of v_i. The lines are least-squares fits to the data. (b) Enlargement of (a) with the addition of rate constants computed from quasiclassical trajectories on the *ab initio* potential surface (open symbols).

part by the small size of missing rate constants in the wings of the distributions. For $v_i \leqslant 12$, sufficient measurements of rate constants with $|\Delta v|>2$ were made that their small contribution to the vibrationally inelastic rate constant k_V was well determined. For $v_i>12$, however, worsening signal to noise conspired with the increased importance of unmeasured rate constants with $|\Delta v|>2$ to make the task of estimating k_V difficult, so that we report only lower bounds to the total rate constants for $v_i = 17$ and 24. Generous error estimates were associated with interpolated and extrapolated data. The resulting rotationally summed rate constants are given in Table I and shown graphically in Fig. 11.

The total vibrationally inelastic rate constant k_V is small at low v_i. It has the value 7.25×10^{-11} cm s^{-1} at $v_i = 2$, 7% of the total inelastic rate constant k_{total}, and extrapolation to $v_i = 0$ gives a value of 3.5×10^{-11} cm s^{-1}, only 3% of k_{total}. At $v_i = 24$, k_V exceeds 42.0×10^{-11} cm s^{-1}, at least 35% of k_{total}. This lower bound includes no estimate of $k_{|\Delta v|>2}$. Multiple quantum jump rate constants ($|\Delta v|>1$) increase more rapidly than single quantum jump rate constants (in a relative but not an absolute sense): the rate constant for $\Delta v = -1$ increases by a factor of 3.7 as v_i increases from 2 to 17, while the $\Delta v = -2$ rate constant increases by a factor of 7.8. Rate constants for individual values of Δv are linear in v_i to within experimental uncertainty [see Fig. 11(a)]. For $\Delta v = \pm 1$, this linearity is consistent with the prediction of one-dimensional perturbative models.[53] It has also been seen in IF $B^3\Pi(0^+)$ - rare gas collisions.[50] However, the observed slope of the $\Delta v = -1$ rate constants cannot persist down to $v_i = 0$, as this rate constant must be zero there.

Total vibrationally inelastic rate constants calculated from quasiclassical trajectories on the *ab initio* potential surface agree in overall magnitude with the measurements but have a different v_i dependence [see Fig. 11(b)]. The rate of increase of the calculated rate constants for $\Delta v = \pm 1$ is sharply higher than that of the measurements: calculated rate constants are lower at low v_i but higher above $v_i = 4$. In contrast, calculated rate constants increase more slowly than measured rate constants for $\Delta v = \pm 2$. It is possible that at least part of the discrepancy is due to failed trajectories at the highest energies, where regions are sampled in which the Alexander–Werner potential is not valid, but in which most of the strong collisions that lead to large changes in v occur. Also, the calculated rate constants for $\Delta v = \pm 2$ exhibit upward curvature above $v_i = 4$, whereas the measured rate constants do not. In fact, the linearity of these experimental rate constants seems remarkable in light of the results of perturbation theory, which would lead one to expect a quadratic dependence on v_i of the $\Delta v = \pm 2$ rate constants.

The total inelastic rate constant k_{total}, (the sum of rotationally and vibrationally inelastic rate constants) is constant

to within experimental error through $v_i = 12$; the steady decline in the rotationally inelastic rate constant is offset by the increase in the vibrationally inelastic rate constant. At $v_i = 17$ and 24, our total rate constants are lower bounds as noted above, but it is clear that these values are at least ten percent larger than the values at lower v_i. This increase in total inelastic scattering coincides with the v_i value at which the average diatom internuclear separation begins a sharp increase (see Fig. 5).

It is easily shown that first-order time-dependent perturbation theory predicts a vibrationally inelastic rate constant for $|\Delta v| = 1$ that increases linearly with increasing v_i for collinear collisions. The exponentially repulsive intermolecular potential is expanded in powers of the separation between the atom and the end of the molecule, which depends on r. Matrix elements of r connecting adjacent vibrational levels depend on the square root of v, and hence the transition probability is linear in v to lowest order in r. This is the essence of the Landau–Teller semiclassical approach,[1,51] which has formed the basis for later, more elaborate perturbative collinear treatments.[52,53] A nonperturbative and more intuitively appealing model of the role of reagent vibration in vibrational transfer has been offered by Nesbitt and Hynes.[54] Building on the earlier collinear work of Benson and coworkers,[55] they have pointed out that

(1) At low initial vibration, increased vibration increases the vibrational velocity in the nearly harmonic portion of the well. The result is increased velocity in the encounter between the atom and the end of the molecule, resulting in greater momentum transfer and hence increased vibrational energy transfer;
(2) At intermediate vibration, the rapid vibrational motion "shadows" certain vibrational phases as the end of the molecule rushes out to meet the atom. Phases including the most rapid vibrational motion begin to be lost, resulting in somewhat reduced vibrational energy transfer efficiency;
(3) At the highest vibrational levels, the molecule lingers at its outer turning point, so that collisions occur almost exclusively with the nearly stationary end of the molecule, resulting in drastically reduced vibrational energy transfer efficiency comparable to that at the lowest levels of vibration.

The quantity $\langle \Delta E \rangle$, the net energy transfer averaged over all collisions, is the primary experimentally testable result of the Nesbitt–Hynes model. This quantity is often of interest;[53,54] it is important in determining relaxation times for vibrationally excited species, and is often the most detailed parameter that it is practical to determine in polyatomic systems.[2] Construction of $\langle \Delta E \rangle$ from rotationally summed rate constants according to

$$\langle \Delta E_{v_i} \rangle = \sum_{v_f \neq v_i} (E_{v_f} - E_{v_i}) \frac{k_{v_i \to v_f}}{k_V} \tag{11}$$

will in general give a result quite different from that obtained using the detailed rate constants:

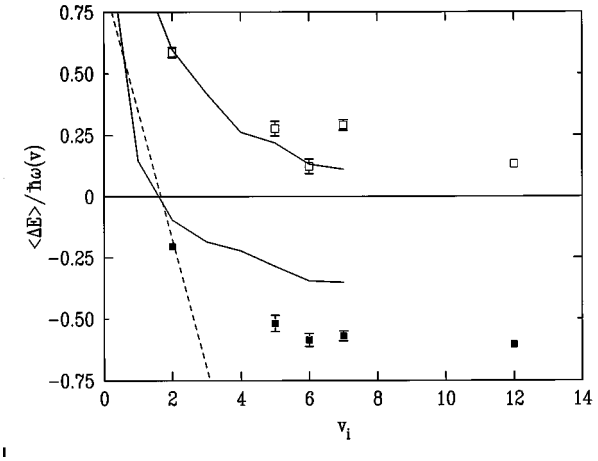

FIG. 12. The net total energy transferred in vibrationally inelastic collisions, scaled by the local oscillator energy spacing, versus v_i. Open squares: net energy transfer computed from level-to-level rate constants [Eq. (12)]. Filled squares: net energy transfer computed from rotationally summed rate constants [Eq. (11)]. Solid lines: results from quasiclassical trajectories on the *ab initio* potential. Dashed line: the simple phase average hard sphere model of Nesbitt and Hynes (Ref. 54).

$$\langle \Delta E_{v_i, j_i} \rangle = \sum_{v_f \neq v_i, j_f} (E_{v_f, j_f} - E_{v_i, j_i}) \frac{k_{v_i, j_i \to v_f, j_f}}{k_V}. \tag{12}$$

Equation (11) is in the spirit of the the measures most often employed, for the simple reason that rotational resolution is usually unavailable. (Our restriction of the sums to vibrationally inelastic rate constants artificially inflates $\langle \Delta E \rangle$ in size but keeps the much larger rotationally inelastic rate constants from swamping the trends we are looking for.) We have computed both these quantities from our experimental data; the results, scaled by the local oscillator spacing, are plotted in Fig. 12 as a function of v_i. The effect of including the rotation explicitly in Eq. (12) is to dramatically shift $\langle \Delta E \rangle$ to more positive values. This occurs because of the shift toward positive Δj of the distributions with $\Delta v < 0$ and because of the quadratic growth with j_f of the rotational energy. For comparison, these averages are displayed for rate constants calculated from trajectories on the *ab initio* surface; the agreement is quite good. Also shown in the figure is the prediction of the simple phase average approximation to the hard sphere model of Nesbitt and Hynes.[54] The one-dimensional model drastically overestimates the amount of energy transfer, as expected,[54] since energy transfer in hard collisions does not suffer the adiabatic reduction that results from impacts with a soft potential. However, the location of the zero in $\langle \Delta E \rangle$ is quite accurately given if comparison is made with the results of Eq. (11), which employ rotationally summed rate constants. It would be interesting to see if this observation holds in other systems; whether it does or not, the *actual* net energy transfer behaves quite differently from that calculated from rotationally summed rate constants.

V. CONCLUSION

We have explored vibrational transfer in the $^7Li_2$ $A^1\Sigma_u^+$ – Ne system with v_i ranging from 2 to 24 and j_i fixed at 30. The range of vibrational term energies spans the lower 57% of the lithium potential, although little more than 20% of the vibrational levels occur within this range. We find simple trends in the rotationally and vibrationally inelastic rate constants.

It would be desirable to extend the results of this work to higher vibrational levels and to other systems through computation and experiment. Computationally, a comparison of the dynamics at various levels of vibrational and rotational excitation for several widely different systems is called for; such a study is feasible now that high quality vibrating potential surfaces are becoming available.[10,56,57] The dynamics of vibrotational transfer on a soft potential is sufficiently complex that no one-dimensional model is likely to quantitatively model the experimental observations with realistic parameters, even though the observations themselves take a simple form. An explicitly three-dimensional model such as the effective mass model of Miklavc and co-workers[49,58] may be able to capture enough of the dynamics to be useful; a quantum mechanical coupled-states calculation would provide a welcome benchmark for comparison with the experimental and quasiclassical results.

Experimentally, the present results may be extended, both in detail and to higher initial vibration. Absolute velocity-dependent cross sections can be measured by a Doppler technique,[13] as can angle-differential cross sections.[16] The decreased averaging of these measurements, particularly the angle-differential cross sections, may permit them to reflect details of the dynamics that are hidden in the present measurements. Extension of this study nearer to dissociation will make possible a rigorous test of the ideas of Nesbitt and Hynes. It will also make it possible to investigate the collisional properties of the fascinating long-range levels of the Li_2 $A^1\Sigma_u^+$ state,[21] as well as the additional dynamical complication of competition with collision induced dissociation. The restrictions that limited the present study to $v_i = 24$ are being removed as a variety of novel techniques, ranging from triple-resonance spectroscopy[19] and fourier transform infrared detection[20] to photoassociative spectroscopy,[59] are mapping out the rest of the A-state vibrational levels and opening a window on their collision dynamics.

ACKNOWLEDGMENTS

We thank Oliver DeWolfe, Jessica Rosenberg, and Mark Rosenberry for assistance in data acquisition and analysis. Acknowledgement is made to the Donors of The Petroleum Research Fund, administered by the American Chemical Society, for the support of this research.

[1] K. F. Herzfeld and T. A. Litovitz, *Absorption and Dispersion of Ultrasonic Waves* (Academic, New York, 1959).
[2] R. J. Gordon, Comments At. Mol. Phys. **21**, 123 (1988).
[3] D. J. Krajnovich, K. W. Butz, H. Du, and C. S. Parmenter, J. Chem. Phys. **91**, 7705 (1989).
[4] D. J. Krajnovich, K. W. Butz, H. Du, and C. S. Parmenter, J. Chem. Phys. **91**, 7725 (1989).
[5] L. Zheng, J. Z. Chou, and G. W. Flynn, J. Phys. Chem. **95**, 6759 (1991).
[6] M. L. Nowlin and M. C. Heaven, J. Chem. Phys. **99**, 5654 (1993).
[7] P. Kusch and M. M. Hessel, J. Chem. Phys. **67**, 586 (1977).
[8] B. Barakat, R. Bacis, F. Carrot, S. Churassy, P. Crozet, F. Martin, and J. Verges, Chem. Phys. **102**, 215 (1986).
[9] G. Baumgartner, H. Kornmeier, and W. Preuss, Chem. Phys. Lett. **107**, 13 (1984).
[10] M. H. Alexander and H.-J. Werner, J. Chem. Phys. **95**, 6524 (1991).
[11] Ch. Ottinger and M. Schröder, J. Phys. B **13**, 4163 (1980).
[12] T. P. Scott, N. Smith, and D. E. Pritchard, J. Chem. Phys. **80**, 4841 (1984).
[13] N. Smith, T. P. Scott, and D. E. Pritchard, J. Chem. Phys. **81**, 1229 (1984).
[14] B. Stewart, P. D. Magill, T. P. Scott, J. Derouard, and D. E. Pritchard, Phys. Rev. Lett. **60**, 282 (1988).
[15] P. D. Magill, T. P. Scott, N. Smith, and D. E. Pritchard, J. Chem. Phys. **90**, 7195 (1989).
[16] T. L. D. Collins, A. J. McCaffery, J. P. Richardson, R. J. Wilson, and M. J. Wynn, J. Chem. Phys. **102**, 4419 (1995).
[17] Y. Gao and B. Stewart, J. Chem. Phys. **103**, 860 (1995).
[18] W. I. McAlexander, E. R. I. Abraham, N. W. M. Ritchie, C. J. Williams, H. T. C. Stoof, and R. G. Hulet, Phys. Rev. A **51**, R871 (1995).
[19] K. Urbanski, S. Antonova, M. Lyyra, A. Yiannopoulou, and W. C. Stwalley, J. Chem. Phys. (in press).
[20] C. Linton, F. Martin, I. Russier, A. J. Ross, P. Crozet, S. Churassy, and R. Bacis, J. Mol. Spectrosc. (in press).
[21] W. C. Stwalley, Contemp. Phys. **19**, 65 (1978).
[22] J. Franck and R. W. Wood, Philos. Mag. **21**, 314 (1911).
[23] J. I. Steinfeld and W. Klemperer, J. Chem. Phys. **42**, 3475 (1965).
[24] Ch. Ottinger, R. Velasco, and R. N. Zare, J. Chem. Phys. **52**, 1636 (1970).
[25] A. N. Nesmeyanov, *Vapor Pressure of the Chemical Elements*, edited by R. Gary (Elsevier, Amsterdam, 1963).
[26] C. R. Vidal and J. Cooper, J. Appl. Phys. **40**, 3370 (1969).
[27] R. N. Zare, *Angular Momentum* (Wiley-Interscience, New York, 1988).
[28] I. Schmidt-Minck, W. Müller, and W. Meyer, Chem. Phys. **92**, 263 (1985).
[29] L. B. Ratcliff, J. L. Fish, and D. D. Konowalow, J. Mol. Spectrosc. **122**, 293 (1987).
[30] W. Preuss and G. Baumgartner, Z. Phys. **A320**, 125 (1985).
[31] I. Schmidt-Minck and W. Meyer, Chem. Phys. Lett. **121**, 49 (1985).
[32] G. Ennen and Ch. Ottinger, Chem. Phys. **41**, 415 (1979).
[33] N. Smith, J. Chem. Phys. **85**, 1987 (1986).
[34] M. Abramowitz and I. A. Stegun, *Handbook of Mathematical Functions* (Dover, New York, 1965).
[35] M. D. Pattengill, in *Atom-Molecule Collision Theory: A Guide for the Experimentalist*, edited by R. B. Bernstein (Plenum, New York, 1979).
[36] M. H. Alexander, A. Berning, A. Degli Esposti, A. Joerg, A. Kliesch, and H.-J. Werner, Ber. Bunsenges. Phys. Chem. **94**, 1253 (1990).
[37] L. K. Cooper, A. J. McCaffery, and S. D. Bosanac, Chem. Phys. Lett. **167**, 233 (1990).
[38] G. Ziegler, S. V. K. Kumar, H. G Rubahn, A. Kuhn, B. Sun, J. Chem. Phys. **94**, 4252 (1991).
[39] W. Müller and R. Schinke, J. Chem. Phys. **75**, 1219 (1981).
[40] See AIP document no. PAPS JCPSA-104-1415-8 for 8 pages of experimental rate constants. Order by PAPS number and journal reference from American Institute of Physics, Physics Auxiliary Publication Service, Carolyn Gehlbach, 500 Sunnyside Boulevard, Woodbury, NY 11797-2999. FAX: 516-576-2223, e-mail: janis@aip.org. The price is $1.50 for each microfiche (98 pages) or $5.00 for photocopies of up to 30 pages, and $0.15 for each additional page over 30 pages. Airmail additional. Make checks payable to the American Institute of Physics.
[41] A. E. DePristo, S. D. Augustin, R. Ramaswamy, and H. Rabitz, J. Chem. Phys. **71**, 850 (1979).
[42] X. Yang and A. M. Wodtke, J. Chem. Phys. **96**, 5123 (1992).
[43] J. A. Barnes, M. Keil, R. E. Kutina, and J. C. Polanyi, J. Chem. Phys. **72**, 6306 (1980).
[44] H.-G. Rubahn, Chem. Phys. **161**, 19 (1992).
[45] H.-G. Rubahn, J. Chem. Phys. **92**, 5384 (1990).
[46] P. D. Magill, B. Stewart, N. Smith, and D. E. Pritchard, Phys. Rev. Lett. **60**, 1943 (1988).
[47] M. M. Maricq, Phys. Rev. A **39**, 3710 (1989).

[49] W. J. Hoving and R. Parson, Chem. Phys. Lett. **158**, 222 (1989).
[50] A. Miklavc, N. Marković, G. Nyman, V. Harb, and S. Nordholm, J. Chem. Phys. **97**, 3348 (1992).
[51] P. J. Wolf and S. J. Davis, J. Chem. Phys. **87**, 3492 (1987).
[52] D. Rapp and T. Kassal, Chem. Rev. **69**, 61 (1969).
[53] R. N. Schwartz, Z. I. Slawsky, and K. F. Herzfeld, J. Chem. Phys. **20**, 1591 (1952).
[54] J. T. Yardley, *Introduction to Molecular Energy Transfer* (Academic, New York, 1980).
[55] D. J. Nesbitt and J. T. Hynes, J. Chem. Phys. **76**, 6002 (1982).
[56] S. W. Benson, G. C. Berend, and J. C. Wu, J. Chem. Phys. **38**, 25 (1963).
[57] J. M. Bowman, J. S. Bittman, and L. B. Harding, J. Chem. Phys. **85**, 911 (1986).
[58] J. M. Hutson, J. Phys. Chem. **96**, 4237 (1992).
[59] T. D. Sewell, S. Nordholm, and A. Miklavc, J. Chem. Phys. **99**, 2567 (1993).
[60] E. R. I. Abraham, N. W. M. Ritchie, W. I. McAlexander, and R. G. Hulet, J. Chem. Phys. **103**, 7773 (1995).